Available online at www.sciencedirect.com

SCIENCE DIRECT®

Biochimica et Biophysica Acta 1607 (2003) 141–151

BIOCHIMICA ET BIOPHYSICA ACTA

BBA

www.bba-direct.com

Properties of mutated *Rhodospirillum rubrum* H^+-pyrophosphatase expressed in *Escherichia coli*

Anders Schultz, Margareta Baltscheffsky*

Arrhenius Laboratories, Department of Biochemistry and Biophysics, Stockholm University, Svante Arrhenius vag 10-12, S-10691 Stockholm, Sweden

Received 31 March 2003; received in revised form 5 September 2003; accepted 12 September 2003

Abstract

The membrane-bound proton pumping inorganic pyrophosphate synthase/pyrophosphatase (H^+-PPi synthase/H^+-PPase) from the photosynthetic bacterium *Rhodospirillum rubrum* was functionally expressed in *Escherichia coli* C43(DE3) cells. Based on a new topology model of the enzyme, charged residues predicted to be located near or within the membrane were selected for site-directed mutagenesis. Several of these mutations resulted in an almost complete inactivation of the enzyme. Four mutated residues appear to show a selective impairment of proton translocation and are thus likely to be involved in coupling pyrophosphate hydrolysis with electrogenic proton pumping. Two of these mutations, R176K and E584D, caused increased tolerance to salt. In addition, the former mutation caused an increased K_m of one order of magnitude for the hydrolysis reaction. These results and their possible implications for the enzyme function are discussed.

Keywords: Inorganic pyrophosphate; Pyrophosphatase; Inorganic pyrophosphate synthase; Proton pumping pyrophosphatase; Phosphohydrolase; *Rhodospirillum rubrum*

1. Introduction

Proton pumping pyrophosphatases (H^+-PPases) are composed of a single 66–116 kDa integral membrane protein with 14–17 predicted transmembrane segments and belong to a fourth category of H^+-phosphohydrolases distinct from F-, V-, and P-ATPases [1–3]. No major amino acid sequence similarity exists between H^+-PPases and any of these other H^+-phosphohydrolases or the soluble pyrophosphatases but there are some similarities between conserved sequence motifs [1,4,5]. H^+-PPases hydrolyze inorganic pyrophosphate (PPi) and use part of the released energy to form a proton gradient [6] over the plasma membrane in prokaryotes [1,7] or various intracellular membranes of organelles such as vacuoles [2–4] and acidocalcisomes [8] in eukaryotes. Recently, it has been shown that H^+-PPases are far more widespread than previously thought [3,9]. They can even, to some extent, replace the soluble PPase [10]. The importance of a H^+-PPase for maintenance of functional acidocalcisomes and growth of *Trypanosoma brucei* has also been demonstrated [11]. Reaction with antibodies [12], sequence comparisons [1], and mutagenesis experiments leading to identification of plausible substrate-binding amino acid residues [5] have revealed a putative active site loop between transmembrane segments 5 and 6 in both plant vacuolar and bacterial H^+-PPases. Results from mutagenesis of *Arabidopsis thaliana* H^+-PPase have revealed other functionally important residues [13].

The H^+-PPi synthase/H^+-PPase activity was first described in chromatophores from the photosynthetic bacterium *Rhodospirillum rubrum* [14,15]. The enzyme from *R. rubrum* catalyzes light-induced formation of PPi from Pi in the chromatophores and is the only known alternative to ATP synthase in biological electron transport phosphorylation. The H^+-PPase from *R. rubrum* is therefore also referred

Abbreviations: PPi, inorganic pyrophosphate; PPase, inorganic pyrophosphatase; H^+-PPase, proton pumping inorganic pyrophosphatase; Rr-H^+-PPase, *Rhodospirillum rubrum* proton pumping inorganic pyrophosphatase; DCCD, *N*,*N*′-dicyclocarbodiimide; EGTA, ethylene glycol-bis(β-aminoethyl ether) *N*,*N*,*N*′,*N*′-tetraacetic acid; FCCP, carbonyl cyanide *p*-(trifluoromethoxy) phenyl hydrazone; FITC, fluorescein 5′-isothiocyanate; PCR, polymerase chain reaction; SDS, sodium dodecyl sulfate; TCA, trichloroacetic acid; TM, transmembrane segment

* Corresponding author. Tel.: +46-8-162-456/000; fax: +46-8-153-679.
E-mail address: meg@dbb.su.se (M. Baltscheffsky).

0005-2728/$ - see front matter © 2003 Elsevier B.V. All rights reserved.
doi:10.1016/j.bbabio.2003.09.003

to as the H^+-PPi synthase. Although the PPi formed in many organisms could merely be a heat-producing hydrolyzable by-product of various biosynthetic reactions, it could serve as an energetic backup system in organisms possessing the H^+-PPase, by maintaining energization of membranes and thereby supporting energy-requiring processes such as secondary transport, ATP synthesis [16], and osmoregulation [2]. In *R. rubrum*, the accumulation of PPi can be as high as 43 mM in illuminated cells [17] in which most of the PPi has been suggested to be in the form of granules [17]. This accumulation could be explained to a major extent by increased PPi production in biosynthesis and down-regulation of the soluble PPase [18], but PPi synthesis by the H^+-PPi synthase may also contribute to some extent. PPi itself has also been shown to serve as an energy and phosphate donor in a number of organisms [19,20] and may have been a predecessor of ATP in early energy metabolism [21].

The cDNA encoding H^+-PPase from *R. rubrum* has been cloned, sequenced [22], and heterologously expressed in *Escherichia coli* [23] and *Saccharomyces cerevisiae* [7] and expressed under a different promoter in *R. rubrum* itself (Schultz and Baltscheffsky, unpublished result).

In this paper, we have expressed the H^+-PPase gene from *R. rubrum* in *E. coli* C43(DE3) cells and have subjected it to site-directed mutagenesis. Amino acid residues apparently important for enzyme activity and for coupling hydrolysis and proton pumping have been identified.

2. Materials and methods

2.1. Plasmid constructions

An original cDNA clone [22] of Rr-H^+-PPase (*R. rubrum* H^+-PPase) was digested with restriction enzymes *Nde*I/*Bam*HI and the released 1400-bp fragment, containing the last two-thirds of the gene, was inserted into pET15b(+) (Novagen) cleaved with the same enzymes. The first part of the gene was amplified from the original cDNA clone by polymerase chain reaction (PCR) using Pfu Turbo DNA polymerase (Stratagene) and primers 1–2 in Table 1. The PCR product was digested with *Nco*I and inserted into the 1400-bp pET15b(+) construct described above. A construct with the inserted PCR fragment in the right orientation was sequenced to confirm absence of any unwanted substitutions. This construct (Rr-H^+-PPase-pET15b(+)) was used to express wild-type Rr-H^+-PPase and as a template for mutagenesis. Mutagenesis was performed by using Stratagene QuikChange™ mutagenesis kit. The primers employed are listed in Table 1. Products of these mutagenesis reactions were digested with either *Bsp*1407I and *Stu*I or *Sgf*I and *Stu*I. Isolated fragments containing the required substitutions were then inserted into the Rr-H^+-PPase-pET15(+) construct, cut with the same enzymes. The inserted regions were sequenced to confirm the presence of the desired mutations and the absence of secondary substitutions.

Table 1
Primers

Substitution	Primers (forward/reverse)
R101K	GGCATGTACATCTCGGTGAAGGCCAATGTGCGCGT-CGCCG
	CGGCGACGCGCACATTGGCCTTCACCGAGATGTAC-ATGCC
R176A	GATCTCGATCTTCGCCGCTCTGGGTGGCGGCATC
	GATGCCGCCACCCAGAGCGGCGAAGATCGAGATC
R176K	GCTGATCTCGATCTTCGCCAAGCTGGGTGGCGGCA-TCTTC
	GAAGATGCCGCCACCCAGCTTGGCGAAGATCGAG-ATCAGC
G178A	GCCCGTCTGGCTGGCGGCATCTTCAC
	GTGAAGATGCCGCCAGCCAGACGGGC
R206A	CCGAGGATGACCCGGCCAATCCCGCCGTCATC
	GATGACGGCGGGATTGGCCGGGTCATCCTCGG
D217A	GACAACGTGGGCGCTAACGTGGGCG
	CGCCCACGTTAGCGCCCACGTTGTC
D217E	GACAACGTGGGCGAGAACGTGGGCG
	CGCCCACGTTCTCGCCCACGTTGTC
E231Q	CCGACCTGTTCCAGACCTATGCCGTG
	CACGGCATAGGTCTGGAACAGGTCGG
E231D	GGCCGACCTGTTCGACACCTATGCCGTGAC
	GTCACGGCATAGGTGTCGAACAGGTCGGCC
K277A	GATCCTCGGCACCGCGTTCGTGAAGCTTGG
	CCAAGCTTCACGAACGCGGTGCCGAGGATC
E351A	GATCTGGGTCACCGCGTATTACACCGGC
	GCCGGTGTAATACGCGGTGACCCAGATC
E351Q	GATCTGGGTCACCCAATATTACACCGGC
	GCCGGTGTAATATTGGGTGACCCAGATC
E351D	GATCTGGGTCACCGACTATTACACCGGC
	GCCGGTGTAATAGTCGGTGACCCAGATC
E385Q	GGCGATTTCGATGCAGGCGACGGCC
	GGCCGTCGCCTGCATCGAAATCGCC
D428N	GGTCGTGGCGCTCAATGCCTATGGTCC
	GGACCATAGGCATTGAGCGCCACGACC
K469A	CCAAGGCGGTGACCGCGGGCTATGCTATCGG
	CCGATAGCATAGCCCGCGGTCACCGCCTTGG
K469D	CCAAGGCGGTGACCGACGGCTATGCTATCG
	CGATAGCATAGCCGTCGGTCACCGCCTTGG
K469R	CCAAGGCGGTGACCCGGGGCTATGCTATCG
	CGATAGCATAGCCCCGGGTCACCGCCTTGG
E584A	GGCGGCGATCAAGGCGATGATCATCCCC
	GGGGATGATCATCGCCTTGATCGCCGCC
E584D	GGCGGCGATCAAGGACATGATCATCCCC
	GGGGATGATCATGTCCTTGATCGCCGCC
G637A	GATCTCGATGACTGCCGCTGGCGGCGCCTGG
	CCAGGCGCCGCCAGCGGCAGTCATCGAGATC
PCR primer 1	GAACCATGGCTGGCATCTATCTT
PCR primer 2	GGATAGGCCATCATCGAGGT

2.2. Expression

E. coli C43(DE3) cells [24] were transformed with wild-type or variant Rr-H^+-PPase-pET15b(+) constructs, and selected for antibiotic resistance on LB plates containing 100 μg/ml ampicillin. A single colony was used to inoculate 3 ml 2 × YT medium [25] supplemented with 100 μg/ml ampicillin (2 × YT-amp) and cells were grown for 10 h at 37 °C and 200-rpm shaking. Then, 0.5 ml of each grown culture was used to inoculate 50 ml of 2 × YT-amp. After 1 h of

incubation at 37 °C and shaking, the cells were induced with 1 mM isopropyl-β-D-thiogalactopyranoside for 6 h and then harvested by centrifugation at 3500 × *g* for 15 min.

2.3. Isolation of inner membrane vesicles (IMVs)

The cell pellets were resuspended in 1 ml of buffer A (20 mM Tris–HCl, 40 μM EGTA, 200 mM KCl, 250 mM sucrose, pH 7.75) supplemented with 5 mM $MgCl_2$, 0.1 mM PPi, and a small amount of lysozyme in microcentrifuge tubes. Resuspensions were allowed to stand at room temperature for 15 min and then chilled on ice before disruption by sonication using Heat Systems Microson™ Ultrasonic Cell Disruptor.

Disruption in ice-water bath was performed in four 30-s pulses (20% output power) with 2-min breaks at an operating frequency of 20 kHz. Unbroken cells and cell debris were removed by two separate centrifugations for 10 min, at 4 °C and full speed (14,000 rpm) in a table microcentrifuge. Supernatants were added to 60 Ti ultracentrifuge tubes filled with 18 ml ice-cold buffer A layered on top of 5 ml buffer A supplemented with 20% sucrose. Membrane fractions were harvested by centrifugation at 150,000 × *g* for 45 min and the IMV pellet was resuspended in 2 ml buffer A by shaking on ice at 4 °C. Resuspended IMVs were subjected to 5-min centrifugation in the microcentrifuge at 4 °C and the supernatant was used for measurements. Protein concentrations in IMV suspensions were measured by the method of Bradford [26]. IMV quantities were calculated in terms of protein content.

2.4. Western blot analysis

IMVs (approximately 1mg/ml) were solubilized by mixing with an equal volume of cold 20 mM Tris–HCl buffer, pH 7.75, containing 0.9 M $MgCl_2$, 50% glycerol, 5 mM dithiothreitol, and 4% Triton X-100. After incubation on ice for 30 min, the same volume loading buffer (0.3 M Tris–HCl, 7% sodium dodecyl sulfate (SDS), 35% glycerol, 0.02% bromophenol blue, pH 6.8) was added and polyacrylamide gel electrophoresis was performed with 12% gels containing 0.1% SDS [27] and 0.8 μg of protein (membrane preparations of wild type and mutants) loaded per lane. After separation, protein bands were transferred electrophoretically to a nitrocellulose membrane and subsequently treated with polyclonal antibodies raised against the H^+-PPase [22]. Antiserum-reactive bands were visualized using an ECL kit (Amersham Biosciences).

2.5. PPi hydrolysis measurements and kinetics

PPi hydrolysis activity was measured by colorimetric estimation of liberated Pi [28] after reaction for 10 min at 30 °C in 0.1 M Tris–HCl, 0.5 mM PPi, 3 mM MgCl2, 40 μM EGTA, 0.5 μM NaF, 2 μM FCCP, pH 7.75. After incubation, samples were chilled on ice and reactions stopped with trichloroacetic acid (TCA)/acetate/formaldehyde (4%/0.5 M/1% final concentrations). Kinetic studies were performed on a few of the mutants in 0.05 M Tris–HCl, 4 mM $MgCl_2$, 0.0125–0.1 mM PPi, 40 μM EGTA, pH 7.2 at 25 °C, using calculated apparent dissociation constants for Mg_2PPi at these conditions [29] for estimation of substrate (Mg_2PPi) concentrations. Michaelis constants for Mg_2PPi hydrolysis of wild type and variants were estimated from Lineweaver–Burk plots.

2.6. Proton translocation measurements

Proton pumping was assayed fluorometrically [5,13,30,38,40,41] using acridine orange (1.5 μM) in 2 ml of buffer A and approximately 50 μg of IMV. Initial rates of proton translocation were estimated as $\Delta F\%\ min^{-1}\ mg^{-1}$ protein, where $\Delta F\%$ = percentage decrease in fluorescence starting at time zero [30]. Steady state acridine orange quenching was measured after 6–10 min (6 μM acridine orange). The excitation and emission wavelengths were set at 495 and 540 nm, respectively. The reaction was initiated by addition of either 0.1 mM PPi or 0.2 mM ATP or 10 mM DL-lactate (sodium salts) and measured with a Perkin Elmer LS 50B fluorescence spectrometer at room temperature (20 °C).

3. Results

3.1. Topological model of R. rubrum H^+-PPase

Five different topology-prediction programs were used to create a model of *R. rubrum* H^+-PPase: Toppred II [31], TMHMM [32], HMMTOP [33], MEMSAT [34], and MPEx (octanol scale) [35]. All programs predicted a highly similar overall topology with all predicted transmembrane helices in the same orientation and with very similarly predicted residue-composition of core regions. One major exception, however, is that TMHMM only predicts 15 transmembrane helices while the other four programs also predict an outwardly oriented transmembrane segment 16 between the C-terminus residues 682–702 (MEMSAT predicted a shorter segment between 681 and 697). Although a majority of predictions support a C-terminus transmembrane helix, the prediction by TMHMM is here favored since a vacuolar H^+-PPase-aequorin fusion protein has been shown to have the aequorin part on the cytosolic side [36]. Assuming no topological change as a result of this fusion, this result suggests a cytosolic location for the C-terminal in the homologous plant vacuolar H^+-PPases [13,36]. In this respect, the TMHMM model is preferred, but it appears to be less compatible with the mutagenesis results presented in this paper compared to the Toppred II model, as will be discussed below. In the Toppred II model, transmembrane 16 is furthermore predicted just above the default cutoff level and can be considered less certain than the other

predicted transmembrane helices. Fig. 1 is based on the Toppred II model with the exception of transmembrane helix 16. Some of the transmembrane helices predicted by this model contain higher amounts of conserved (here defined as present in more than 80% of available sequences from databases) and hydrophilic residues, which indicate a central position in the transmembrane region. Furthermore, helical-wheel analysis reveals an unequal distribution of these residues along the helix axis (Fig. 2) and thus identifies transmembrane helices 3, 5, 10, and 12 as plausible candidates for forming the inner, proton-conducting part of the channel.

3.2. Expression of *R. rubrum* H^+-PPase in *E. coli*

E. coli strain C43(DE3) [24] was transformed with a construct containing the Rr-H^+-PPase gene cloned into pET15b(+) vector under control of the T7/lac promoter. Cells were grown and membrane vesicles isolated as described in Section 2. As Fig. 3 shows, Western blot analysis revealed an immunoreactive band with apparent approximate size of 60 kDa. Although this size differs from the molecular mass calculated from the amino acid sequence (71 kDa), it agrees with prior results [37]. This anomalic migration in SDS-polyacrylamide gels can be explained by the very hydrophobic nature of the Rr-H^+-PPase. No immunoreactive band was seen when cells were transformed with the pET15b(+) vector alone, without Rr-H^+-PPase gene (Fig. 3).

The expressed enzyme was functional with retained sensitivity to imidodiphosphate (IDP), DCCD, FITC, and a characteristic low sensitivity to the typical inhibitor of soluble PPases, fluoride. The pyrophosphatase activity of isolated vesicles was 1.3 μmol min^{-1} mg^{-1} protein, which is considerably higher than in chromatophores isolated from *R. rubrum* [37]. The high expression level is mainly due to the *E. coli* C43(DE3) strain, which is particularly suitable for overexpression of integral membrane proteins [24]. Expression in conventional *E. coli* BL21(DE3) (Novagen) yielded three to four times lower activity. A low level of contaminating *E. coli* soluble pyrophosphatase activity (less than 3% as measured in vesicles from pET15b(+) transformed bacteria) was practically eliminated by addition of 0.5 mM NaF in subsequent activity measurements.

PPi-dependent intravesicular acidification of the expressed enzyme was monitored by acridine orange fluorescence quenching showing an initial rate and steady state (after 6–10 min) of about 1000 $\Delta F\%$ min^{-1} mg^{-1} protein and 1400 $\Delta F\%$ min^{-1} mg^{-1}, respectively. A significant proton gradient was also generated by the intrinsic *E. coli* membrane proteins, F_0F_1-ATPase and D-lactate dehydrogenase upon addition of ATP or lactate, indicating integrity of the vesicles. The pH gradient collapsed in each case by addition of membrane permeable ammonium ions, indicating previous proton transport into the vesicles. A low background fluorescence quenching (less than 1%) was detected in vesicles from bacteria transformed with pET15b(+).

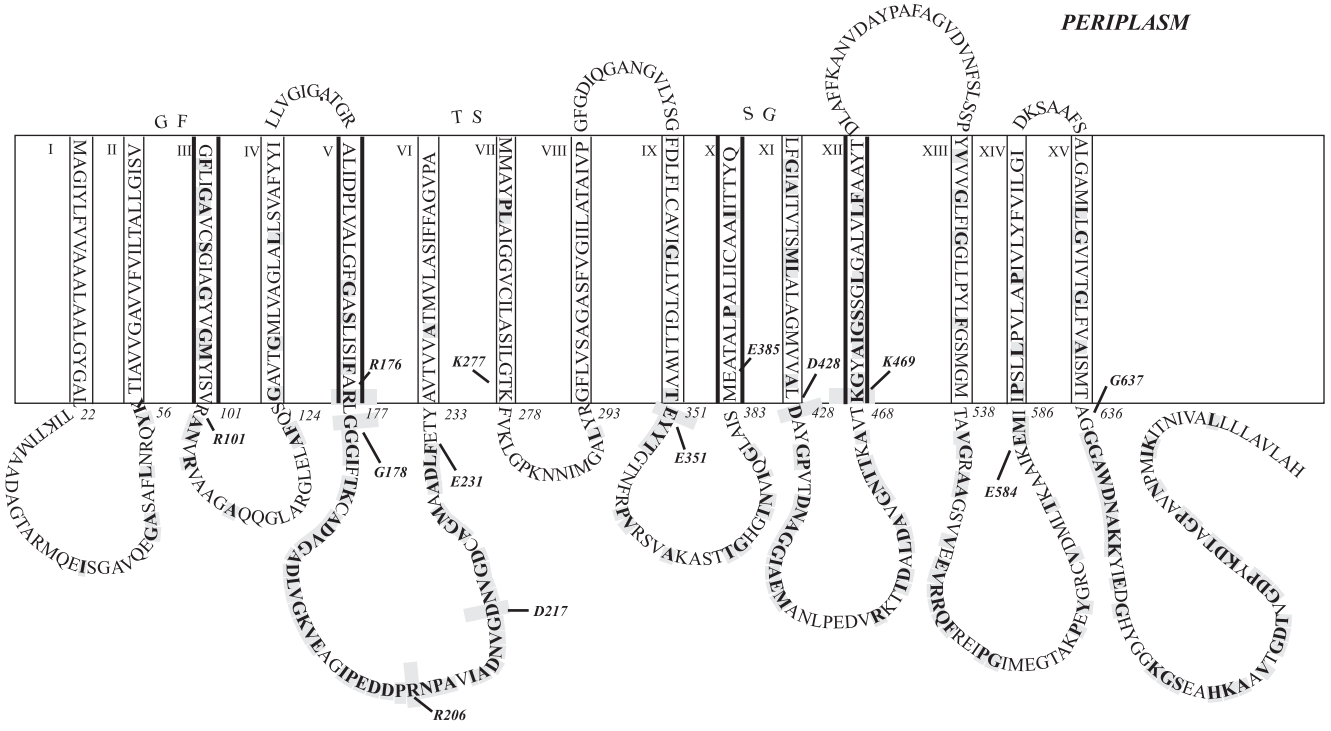

Fig. 1. Topology model based on Toppred II [31] prediction with exception of a putative transmembrane segment 16 between residues 682–702 (see text). Residues selected for mutagenesis are depicted by arrows. Highlighted and bold residues are conserved among available sequence homologues in databases to at least 80% when aligned using Clustal W. Transmembrane helices surrounded with bold lines are likely candidates for forming the inner core of the proton channel as revealed by their amino acid composition and helical wheel analysis (Fig. 2).

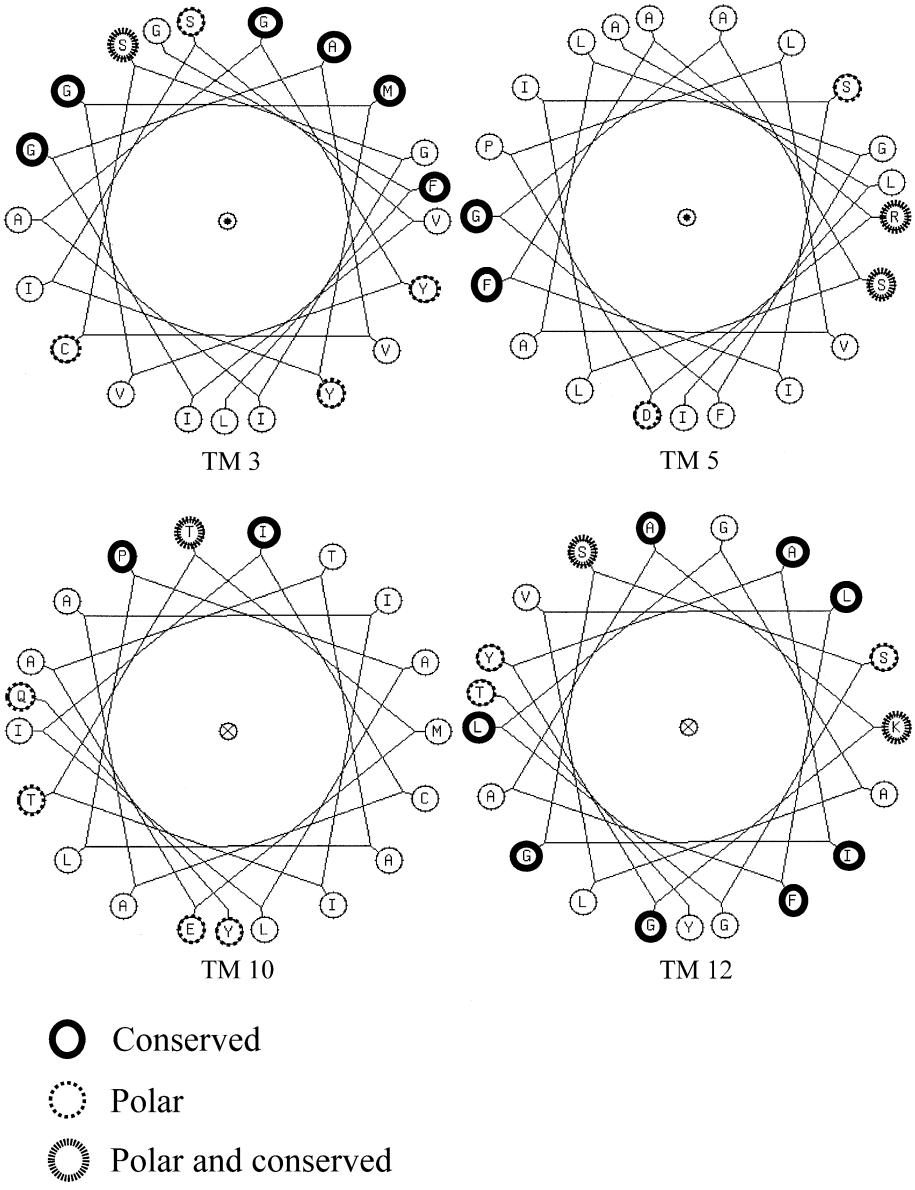

Fig. 2. Helical wheel plots of predicted transmembrane segments (TMs) 3, 5, 10, and 12.

3.3. Site-directed mutagenesis

Targets for mutagenesis were mainly selected among charged residues predicted to be located at the interphase between cytosol and membrane or within the membrane (see Fig. 1 and Section 4), with special attention given to putative membrane-spanning regions containing the highest amounts of hydrophilic residues in the Rr-H^+-PPase as well as a comparatively high degree of conservation in the H^+-PPase family. The charged residues were replaced either with residues of the same charge, alanine residues, or Asn and Gln for Asp and Glu, respectively. In addition, the first glycine residues in each of the two triple-G motifs, proposed as plausible flexible regions that may support a conformational change mechanism [1], were changed to alanine residues. The word motif is used here for highly conserved sequence patterns of assumed importance for enzyme function. Western blot analysis (Fig. 3) showed that all mutants were expressed at approximately the same level as the wild type.

Activity measurements revealed a group of mutants almost completely deficient in both PPi-dependent proton translocation and PPi hydrolysis (see Table 2). In this group, we find variants E231D, E231Q of an acidic (E231) residue and R176A of a basic (R176) residue predicted to be located in the membrane-cytosol interphase flanking the putative active-site loop. All three variants, K469A, K469D, K469R, of the highly conserved K469 (present in all homologues found by us in databases) belong here too. In this group, we also see substitutions D217A, D217E of D217, located in the putative active-site loop [1,5,12] and D428N of D428, whose corresponding residues have earlier been identified as

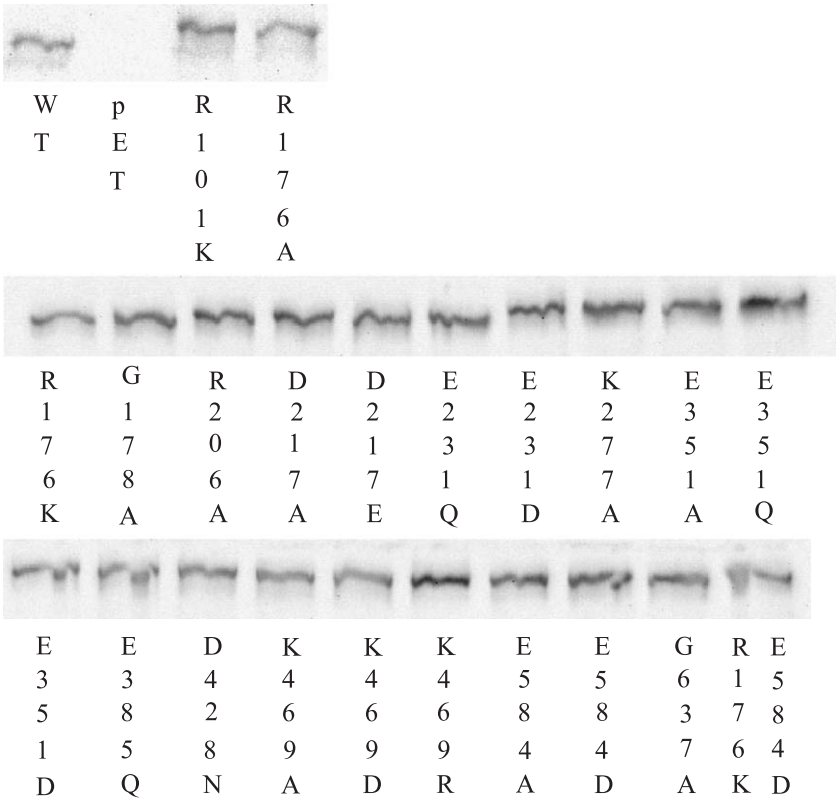

Fig. 3. Western blots of wild type and the expressed mutants. Membrane preparations were subjected to gel electrophoresis. Protein bands were transferred to and immobilized on a nitrocellulose filter, subsequently treated with antibodies raised against the H^+-PPase. WT is wild type and pET is a Western blot of bacteria transformed with vector only.

functionally important in *Vigna radiata* [5] and *A. thaliana* [13], respectively.

A second group of mutants appear to exhibit selective impairment of proton translocation, which make the mutated residues plausible candidates for being involved in coupling hydrolysis with proton translocation. Among them are R176K and the alanine substitution of the first glycine residue in the triple-G motif within the putative active-site loop [1,5,12]. Variants E351A, E351D, E351Q, E584A, E584D of two glutamate residues (E351 and E584) also belong to this group (Table 2). A double mutant of R176K and E584D retains less than a tenth of the hydrolysis activity and shows no detectable proton pumping. A glutamine substitution of the glutamate residue in *A. thaliana* corresponding to E351 has earlier been shown to also affect proton pumping more, but an aspartate substitution of that glutamate residue shows increased activity as compared to the wild type [13]. On the contrary, an E351D variant of the *R. rubrum* enzyme shows only half the wild-type hydrolysis activity and even less proton pumping. Notably, the differences in steady state acridine orange quenching (given within brackets for some of the mutants in Table 2) are less pronounced than when initial quenching rates of wild type and this second group of mutants are compared. This will be discussed below. Also, all the variants of E231, D428, K277, and K469 appear to show some selective impairment of proton translocation, but here the differences are quite small. To measure pH gradients and proton translocation by using acridine orange has been questioned [38]. In an attempt to test the method, initial rates and steady state (after 6–10 min) acridine orange quenching were measured for wild-type and plotted against sample size (Fig. 4). The plots show a close to linear relationship between sample size and both initial rates and steady state quenching of acridine orange in the range tested.

The remaining mutants retain more than half of the wild-type activity of both hydrolysis and proton pumping. Approximate Michaelis constants (K_m) for pyrophosphate hydrolysis were estimated using Lineweaver–Burk plots of wild-type enzyme and a few variants. K_m of the wild-type enzyme was estimated to be 15 μM, about the same value for G178A, half this value for E564D and an order of magnitude higher for R176K.

3.4. Effects of salt and pH

The wild-type tolerates a wide range of NaCl concentrations. The highest rate of pyrophosphatase activity under the conditions used is reached at pH 7.75.

Salt tolerance is further increased in the R176K and E584D variants of the enzyme and still further in the double mutant (see Fig. 5). Testing at least one membrane prepa-

Table 2
Effects of substitution of residues on activities of heterologously expressed *R. rubrum* H^+-PPase

Substitution	H^+ translocation	PPi hydrolysis	Ratio of activities
	Percent of wild type	Percent of wild type	ΔF% μmol^{-1} PPi hydrolyzed
Wild type	100 ± 15	100 ± 13	770
R101K	130 ± 10	130 ± 11	770
R176A	N.D.	4 ± 2	N.A.
R176K	22 ± 4.5 (32)	48 ± 7	350
G178A	12 ± 2.5 (25.5)	51 ± 8	180
R206A	72 ± 7	90 ± 10	620
D217A	N.D.	3 ± 1	N.A.
D217E	N.D.	1.5 ± 1	N.A.
E231Q	N.D.	3 ± 1	N.A.
E231D	N.D.	5 ± 1	N.A.
K277A	60 ± 10 (82)	90 ± 12	510
E351A	50 ± 5 (68)	80 ± 10	480
E351Q	23 ± 4 (33)	43 ± 5	410
E351D	30 ± 5	52 ± 7	440
E385Q	55 ± 12 (80)	60 ± 11	710
D428N	N.D.	3 ± 1	N.A.
K469A	N.D.	2 ± 1	N.A.
K469D	N.D.	2 ± 1	N.A.
K469R	4 ± 2	7 ± 2	440
E584A	30 ± 5	55 ± 8	420
E584D	11 ± 2.5 (21.5)	35 ± 5	240
G637A	52 ± 5	54 ± 8	740
R176K/E584D	N.D.	8 ± 2	N.A.

Percentage of activities compared to wild-type activity are given. H^+ translocation activity is given as initial rates of acridine orange quenching (1000 ± 110 ΔF% min^{-1} mg^{-1} protein for wild type). Steady state acridine orange quenching measured on a single membrane preparation is given within brackets for some of the mutants (1400ΔF% mg^{-1} protein for wild type). Hydrolysis activity was measured as the amount of Pi liberated after 10-min incubation at 30 °C (1.3 μmol min^{-1} mg^{-1} protein for wild type). The "ratio of activities" is the ratio of H^+ translocation activity (ΔF% min^{-1} mg^{-1} protein) and hydrolysis activity (μmol min^{-1} mg^{-1} protein). Activity measurements were performed at least twice on each of two to four different membrane preparations of each variant. The figures in this table are mean values of these measurements and are given as percentage, with standard deviations, of the reference wild-type activity. Each time membrane preparations of mutants were made (three to five at a time), a membrane preparation of the wild type was made as a reference. N.D. = not detectable. N.A. = not applicable.

ration of a few other mutants (R101K, R206A, K277A E351A, E351D, and K469R) showed salt tolerances equal to or somewhat lower than the salt tolerance recorded for the wild-type enzyme. The activity values for R176K and E584D (in percent as compared to the activity in the absence of salt) are mean values with standard deviations of measurements on four different membrane preparations (Fig. 5). The relative activities of R176K, E584D and their double mutants were significantly different from wild-type activities at 0.4 and 0.6 M NaCl ($P < 0.01–0.05$ Student's *t*-test). The inhibitory effect seems to be exerted by the sodium ions since appropriate concentrations of Na_2SO_4, but not of KCl, have similar effects on the activity (data not shown).

The E584D variant appears to show a somewhat higher relative activity at pH 6.5 compared to wild type when both are compared to their hydrolytic activities at pH 7.75 (98% and 71%, respectively). The percentage figures are mean values of measurements on four different membrane preparations but are barely significantly different ($P < 0.1$ Student's *t*-test). If the 90% confidence level indicates that a

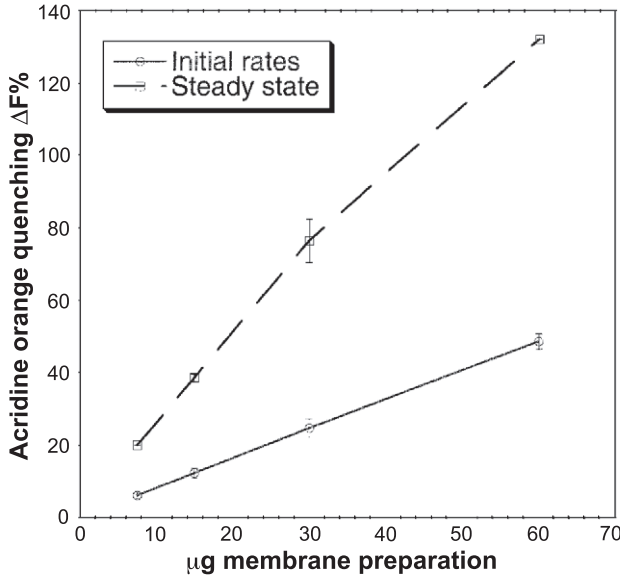

Fig. 4. Acridine orange quenching, measured as described in Section 2, plotted against amount of membrane preparation of bacteria expressing the wild-type H^+ PPase. Initial rates and steady state (after 6–10 min) acridine orange quenching were measured. Results, with standard deviations, are based on measurements on two different membrane preparations of bacteria expressing wild-type H^+-PPase.

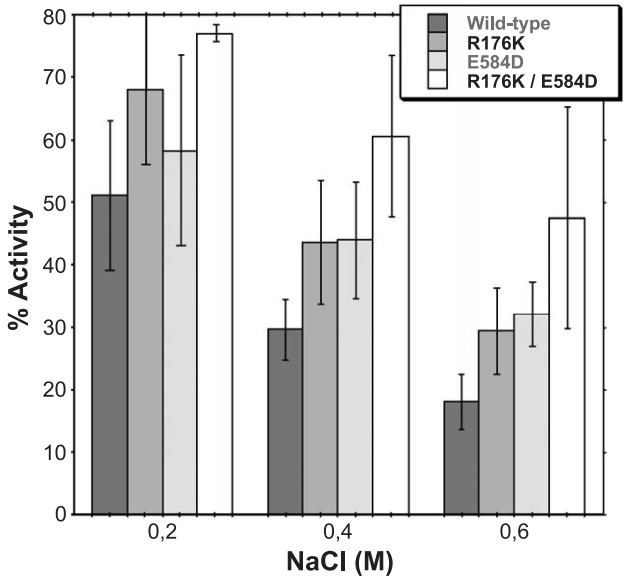

Fig. 5. Sensitivity of wild type and mutant H^+-PPases to NaCl. Activities are plotted against concentration of NaCl (M). One hundred percent activity is the activity obtained in the absence of added NaCl. Absolute activities are given in Table 2. Results given are mean values with standard deviations of measurements on four (wild type, R176K, and E584D) or two (double mutant R176K/E584D) different membrane preparations. Relative activities of R176K and E584D are significantly different from wild type at 0.4 and 0.6 M NaCl ($P < 0.01–0.05$% paired Student's *t*-test).

true difference exists, it may reflect the lower pK_a of the side chain of aspartate as compared to that of glutamate.

4. Discussion

The topological model (Fig. 1) shows, in agreement with early experimental results [39], a highly hydrophobic enzyme with almost half of its residues predicted to be located within the membrane. The predictions by five different topology prediction programs are essentially the same but there are a few notable differences: First, a majority of programs predict a transmembrane segment 16, but biochemical evidence favors a cytosolic location of the C-terminus [13,36]. Another important difference is the predicted length of transmembrane segment 5. Two of the programs (TMHMM and MEMSAT) predict the triple-G motif to be located within the membrane, but this seems unlikely since both R176A and G178A strongly affect hydrolysis activity. Furthermore, arginine residues are seldom located in the inner regions of membranes and from that position the substitution to lysine in the R176K mutant is unlikely to have a strong effect on the K_m for pyrophosphate hydrolysis of the enzyme.

R176 with its positive charge could possibly be a topological determinant ensuring the right location of the potentially flexible GGG-region, but it may also have other important functions as discussed below. Interestingly, when changing this R to an A, all tested programs predict an inside-membrane location of GGG. All programs predict the functionally important E231, E351, D428, K469, and E584 to be very close to the membrane, possibly in the interphase region. Charged residues (as they appear in water and at neutral pH) are, however, almost totally absent in the central part of any predicted transmembrane helix. Three of the programs predict E385 to be an exception, but both measured activities of the E385Q variant do not suggest a crucial role for this residue (Table 2).

Other results from the mutagenesis analysis reveal a group of mutants with almost no activity at all, which indicate crucial structural or mechanistic functions of the changed residues. Inhibition studies with DCCD and FITC (in preparation) identified two of these residues as main targets and protection studies with substrate indicated that they both are involved in substrate binding. The probable main target for DCCD, D217, is the middle aspartate in the strongly conserved DNVGDNVGD motif in the putative active site loop [1,5,12] of H^+-PPases and the target for FITC is the also highly conserved K469, which is the first residue in the most conserved and hydrophilic transmembrane segment predicted (the five topology programs used predict it to be located either as the first residue of TM12 or 1–2 residues before the start). This location of K469 and the reaction of the hydrophobic DCCD with D217 agree with a closeness of the substrate-binding site to the membrane regions.

Another highly conserved region, DVGADLVGKVE, contains sequence similarity to the well-known P-loop motif of ATPases [1] and has in plant vacuolar H^+-PPases been shown to have substrate-binding residues as indicated by mutagenesis experiments and protection studies with trypsin [5]. Mutagenesis experiments in *V. radiata* have shown that substitutions of at least three of these residues (V193A, K195R, and E197D; *R. rubrum* numbering) result in an enzyme with partly retained hydrolysis activity but with complete loss of proton translocation [5]. This could be interpreted as a requirement for optimal binding to allow conservation of released energy as a proton gradient. Conservation of energy could possibly be mediated through conformational change. The potentially flexible GGG motif, a few residues before DVGADLVGKVE in the active-site loop, may be necessary to allow optimal performance of such a change. A mutation of the first glycine residue in this triplet (G178A) affects especially proton pumping strongly, but it does not appear to affect substrate binding since the Michaelis constant remains approximately the same as in the wild type. A substitution of the first G in the second GGG triplet (G637 of the loop after transmembrane segment 15) affects, on the other hand, both measured activities equally much.

Mutants of at least four amino acid residues (R176, G178, E351, and E584) presented in this paper appear to exhibit selective impairment of proton translocation, which indicates their involvement in energy coupling. One of them is the first glycine residue in the GGG-motif mentioned above and another is E351, which is present in the conserved motif EYYT. A glutamine substitution of the corresponding glutamate residue in *A. thaliana* (E427, *A. thaliana* numbering) has also been shown to effect proton translocation more than hydrolysis activity [13]. However, in this case, an activation of the enzyme occurs after substitution by an aspartate, whereas activities remain low in this variant of the *R. rubrum* enzyme. Furthermore, the ratio of proton pumping activity and hydrolysis activity of an *A. thaliana* H^+-PPase variant with its E427 replaced by Q is considerably lower than what is the case for the E351Q variant of *R. rubrum* H^+-PPase. These results may reflect a somewhat different organization of residues at the entrance of the proton-conducting channel that could be important for function.

The use of acridine orange for estimation of proton gradients and proton translocation has been questioned since it has been shown that temperature and anions affect the accumulation of acridine orange into vesicles [38]. Nevertheless, a linear relationship between acridine orange quenching and ΔpH has been shown to occur under fixed experimental conditions and at a limited pH range [40], the uncertainty increasing at low ΔpH [41]. In an attempt to investigate if a linear relationship between proton pumping and acridine orange quenching can be assumed under the conditions used in this study, both initial rates and steady state acridine orange quenching were plotted against the

amount of wild-type membrane preparation (Fig. 4). The plots, based on measurements on two membrane preparations, are close to linear, which indicates that the results of proton translocation measurements (Table 2) may significantly be compared with each other. However, many mutants show some degree of stronger inhibition of proton pumping as compared to pyrophosphate hydrolysis (Table 2). Another point of concern is the observation that the differences in steady state acridine orange quenching (given within brackets for some of the mutants in Table 2) are less pronounced than when initial quenching rates of wild type and the second group of mutants (those that appear to show selective impairment of proton pumping) are compared. If the stronger effects on initial rates reflect actual slower proton pumping rates or can be considered as experimental artifacts may be an open question. Here the former interpretation is favored since the wild-type initial rates of fluorescence quenching seem to be proportional to the amount of tested membrane preparation (Fig. 4). It appears that the extent of uncoupling in the mutants is larger in the initial phase when the proton gradient still is small, allowing a higher reaction rate.

The percent figures for steady state quenching of R176K and E351D in Table 2 seem (in apparent contradiction to the results obtained when initial quenching rates and pyrophosphate hydrolysis were compared) to be close to the corresponding figures for pyrophosphate hydrolysis in the same table. When comparing these data, one has to be aware of that the hydrolysis measurements were performed in an uncoupled system (in the presence of FCCP) after 10-min reaction, whereas proton-pumping measurements were made continuously without uncoupler. In the absence of an uncoupler, the difference in pyrophosphate hydrolysis (when measured as described above) between wild type and mutants is generally smaller since the wild type in most of the cases reaches steady state quicker. Therefore, measurements of pyrophosphate hydrolysis in the presence of an uncoupler give a better estimate of the effect of mutations. A comparison between initial rates and uncoupled hydrolysis is more correct in that sense because the formed proton gradient still is small during the initial phases. Thus, an ideal comparison is only possible when both activities are measured simultaneously, but a technical solution for this has not been available to us.

E584D and R176K also belong to this category of mutants with apparently stronger inhibition of proton translocation than of pyrophosphate hydrolysis. In addition, they show decreased sensitivities to salt (Fig. 5). The E584D mutant may also have a somewhat shifted pH profile as compared to the wild type (Section 3.4) and has a low ratio of proton pumping activity and pyrophosphate hydrolysis (Table 2). R176 may also be important since the K_m for pyrophosphate hydrolysis of R176K is an order of magnitude higher as compared to the wild type, which may indicate that R176 is involved in substrate binding. The decreased sensitivities to salt of these mutants may possibly be relevant in connection with a recently proposed mechanism of *E. coli* proton-translocating transhydrogenase [42].

In that enzyme, the membrane domain (dII) and the NADP(H) binding domain (dIII) are connected through a highly conserved peptide linker (the dII–dIII linker). An aspartate residue, D213, in a loop adjacent to the dII–dIII linker has been shown to be important for proton translocation and to be close enough to form a salt bridge with an arginine residue (R265) in the dII–dIII linker. It has been proposed that this salt bridge is formed and broken as a means to mechanistically transfer conformational changes in dII to dIII via a "pulling effect" on the dII–dIII linker. In a model of the reverse reaction, NADPH binds to dIII and causes a conformational change that increases the pK_a of D213, which then leads to a splitting of the salt bridge when it binds a proton. Breakage and establishment of this salt bridge is believed to favor the occluded and open state, respectively, of the NADP(H) site in dIII [42].

The idea that such a salt bridge may be involved in the coupling of an energetically favorable reaction with proton pumping may also be worth considering for the H^+-PPase,

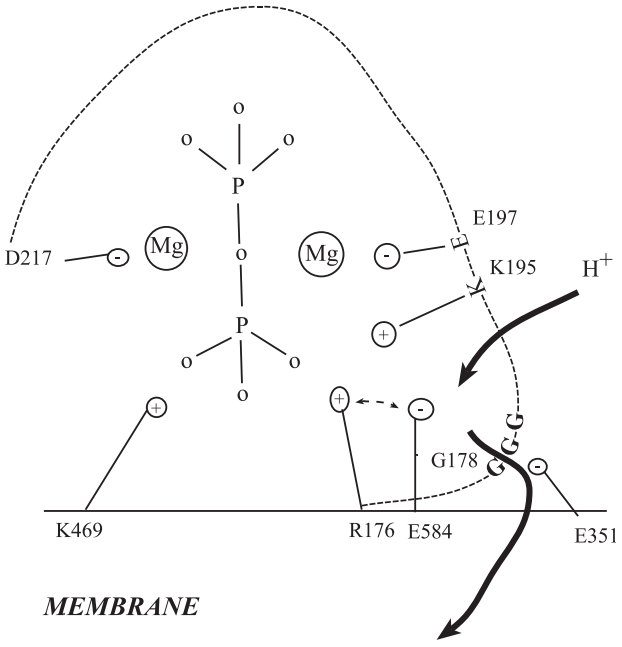

Fig. 6. A tentative outline of a putative active site of H^+-PPases. Amino acid residues (marked with *R. rubrum* numbering) within the putative active site loop (the loop between transmembrane helices 5 and 6 in *R. rubrum*) are connected with a dashed line. Amino acid residues corresponding to K195, E197, and D217 have previously been proposed as substrate binding in *V. radiata* [5]. In addition, the two former residues show selective impairment of proton pumping [5]. The counterpart of E351 has also been shown to be important for coupling of pyrophosphate hydrolysis with proton-translocation in *A. thaliana* [13]. Our data indicate that R176, G178, E351, and E584 may be important for coupling in *R. rubrum* and R176 also in substrate binding. The possible substrate binding roles of D217 and K469 are briefly treated in the discussion. A number of other residues mutated here and in other reports [5,13] were essential for enzyme function, but their roles are as yet less clear. R176 and E584 may be involved in salt bridge(s), either with each other or with unknown residues (see Section 4).

although structurally unrelated to transhydrogenases. Given the decreased sensitivities to salt of E584D and R176K, it is tempting to speculate that a salt bridge may be formed between E584 and R176. High salt concentration is likely to interfere with this putative salt bridge in the wild type, but has less effect on a mutant with an already broken salt bridge. However, a major role for this putative salt bridge may be contradicted by the fact that the E584A mutant retains as much as approximately half of the hydrolysis activity and 30% of the proton pumping (Table 2). Further decreased salt sensitivity of the double mutant R176K/E584D (Fig. 4) may indicate that each of these residues may alternatively form salt bridges with as yet unidentified amino acid residues. R176 may in that case be involved in a salt bridge of functional importance since R176A in contrast to E584A has almost no retained activities. However, this speculation could be contradicted by the small (although statistically significant) difference in salt sensitivity of R176K as compared to the wild-type enzyme (Fig. 5), since a larger difference may be expected if the putative salt bridge is functionally important. An alternative explanation for these rather small differences may be that when a functionally important salt bridge is broken, it is replaced by another salt bridge. Herewith a picture of a possible network of charged residues, which could be advantageous from an evolutionary point of view, appears to have emerged. A clarification of this situation needs further experimentation.

In conclusion, Fig. 6 shows a model based on our data and results from previous reports [5,13]. Some amino acid residues (connected by a dashed line in Fig. 6) present in the putative active site loop may be important for hydrolysis activity as well as for coupling. Lacking 3D structural information about the H^+-PPase, the model is proposed as a possible object for further discussion and experimentation.

Acknowledgements

Support from Carl Tryggers Stiftelse för Vetenskaplig Forskning and Magnus Bergvalls Stiftelse is gratefully acknowledged. We thank Professor J.E. Walker for providing the *E. coli* C43(DE3) strain and Professors H. Baltscheffsky, R. Lahti and Mr. G.A. Belogurov for valuable discussions.

References

[1] M. Baltscheffsky, A. Schultz, H. Baltscheffsky, H^+-PPases: a tightly membrane-bound family, FEBS Lett. 452 (1999) 121–127.
[2] M. Maeshima, Vacuolar H^+-pyrophosphatase, Biochim. Biophys. Acta 1465 (2000) 37–51.
[3] Y.M. Drozdowicz, P.A. Rea, Vacuolar H^+-pyrophosphatases: from the evolutionary backwaters into the mainstream, Trends Plant Sci. 6 (2001) 206–211.
[4] P.A. Rea, Y. Kim, V. Sarafian, J.M. Davies, R.J. Poole, D. Sanders, Vacuolar H^+-translocating pyrophosphatases: a new category of ion translocase, Trends Biochem. Sci. 17 (1992) 262–266.
[5] Y. Nakanishi, T. Saijo, Y. Wada, M. Maeshima, Mutagenic analysis of functional residues in putative substrate-binding site and acidic domains of vacuolar H^+-pyrophosphatase, J. Biol. Chem. 276 (2001) 7654–7660.
[6] J. Moyle, R. Mitchell, P. Mitchell, Proton-translocating pyrophosphatase from *Rhodospirillum rubrum*, FEBS Lett. (1972) 233–236.
[7] J.R. Pérez-Castinera, R.L. Lopez-Marques, M. Losada, A. Serrano, A thermostable K^+-stimulated vacuolar-type pyrophosphatase from the hyperthermophilic bacterium *Thermotoga maritima*, FEBS Lett. 496 (2001) 6–11.
[8] M.T. McIntosh, A.B. Vaidya, Vacuolar type H^+ pumping pyrophosphatases of parasitic protozoa, Int. J. Parasitol. 32 (2002) 1–14.
[9] J.R. Pérez-Castinera, R. Gómez-García, R.L. Lopez-Marques, M. Losada, A. Serrano, Enzymatic systems of inorganic pyrophosphate bioenergetics in photosynthetic and heterotrophic protists: remnants or metabolic cornerstones? Int. Microbiol. 4 (2001) 135–142.
[10] J.R. Pérez-Castinera, R.L. Lopez-Marques, J.M. Villalba, M. Losada, A. Serrano, Functional complementation of yeast cytosolic pyrophosphatase by bacterial and plant H^+-translocating pyrophosphatases, Proc. Natl. Acad. Sci. U. S. A. 99 (2002) 15914–15919.
[11] G. Lemercier, S. Dutoya, F.A. Ruiz, C.O. Rodrigues, T. Baltz, R. Docampo, N. Bakalara, A vacuolar type H^+-pyrophosphatase governs maintenance of functional acidocalcisomes and growth of the insects and mammalian forms of *Trypanosoma brucei*, J. Biol. Chem. 277 (2002) 37369–37376.
[12] A. Takasu, Y. Nakanishi, T. Yamauchi, M. Maeshima, Analysis of the substrate binding site and carboxyl terminal region of vacuolar H^+-pyrophosphatase of mung bean with peptide antibodies, Biochem. J. 122 (1997) 883–889.
[13] R.G. Zhen, E.J. Kim, P.A. Rea, Acidic residues necessary for pyrophosphate-energized pumping and inhibition of the vacuolar H^+-pyrophosphatase by *N*,*N*′dicyclohexylcarbodiimide, J. Biol. Chem. 272 (1997) 22340–22348.
[14] H. Baltscheffsky, L.-V. Von Stedingk, H.W. Heldt, M. Klingenberg, Inorganic pyrophosphate: formation in bacterial photophosphorylation, Science 153 (1966) 1120–1122.
[15] M. Baltscheffsky, Inorganic pyrophosphate and ATP as energy donors in chromatophores from *Rhodospirillum rubrum*, Nature 216 (1967) 241–243.
[16] D.L. Keister, N.J. Minton, ATP synthesis driven by inorganic pyrophosphate in *Rhodospirillum rubrum* chromatophores, Biochem. Biophys. Res. Commun. 42 (1971) 932–939.
[17] G.F. Salih, P. Nyrén, Determination of the intracellular concentration of inorganic pyrophosphate in *Rhodospirillum rubrum*, Curr. Res. Photosynth. 3 (1990) 209–212.
[18] J.-H. Klemme, H. Gest, Regulation of the cytoplasmic inorganic pyrophosphatase of *Rhodospirillum rubrum*, Eur. J. Biochem. 22 (1971) 529–537.
[19] M. Stitt, Pyrophosphate as an energy donor in the cytosol of plant cells: an enigmatic alternative to ATP, Bot. Acta 111 (1998) 167–175.
[20] M. Baltscheffsky, P. Nyrén, The synthesis and utilization of inorganic pyrophosphate, in: L. Ernster (Ed.), Bioenergetics, Elsevier, Amsterdam, 1984, pp. 187–206.
[21] H. Baltscheffsky, Major "anastrophes" in the origin and early evolution of biological energy conversion, J. Theor. Biol. 187 (1997) 495–501.
[22] M. Baltscheffsky, S. Nadanaciva, A. Schultz, A pyrophosphate synthase gene: molecular cloning and sequencing of the cDNA encoding the inorganic pyrophosphate synthase from *Rhodospirillum rubrum*, Biochim. Biophys. Acta 1364 (1998) 301–306.
[23] G.A. Belogurov, M.V. Turkina, A. Penttinen, S. Huopalahti, A.A. Baykov, R. Lahti, H^+-pyrophosphatase of *Rhodospirillum rubrum*: high-yield expression in *Escherichia coli* and identification of the cys residues responsible for inactivation by mersalyl, J. Biol. Chem. 277 (2002) 22209–22214.

[24] B. Miroux, J.E. Walker, Overproduction of proteins in *Escherichia coli*: mutant hosts that allow synthesis of some membrane proteins and globular proteins at high levels, J. Mol. Biol. 260 (1996) 289–298.
[25] J. Sambrook, E.F. Fritsch, T. Maniatis, Molecular Cloning: A Laboratory Manual, 2nd ed., Cold Spring Harbor Laboratory Press, Cold Spring Harbor, NY, 1989.
[26] M.M. Bradford, A rapid and sensitive method for the quantitation of microgram quantities of protein utilizing the principle of protein–dye binding, Anal. Biochem. 72 (1976) 248–254.
[27] U.K. Laemmli, Cleavage of structural proteins during the assembly of the head of bacteriophage T4, Nature 227 (1970) 680–685.
[28] W.B. Rathbun, V.M. Betlach, Estimation of enzymatically produced orthophosphate in the presence of cysteine and adenosine triphosphate, Anal. Biochem. 28 (1969) 436–445.
[29] S.E. Volk, A.A. Baykov, V.S. Duzhenko, S.M. Avaeva, Kinetic studies on the interactions of two forms of inorganic pyrophosphatase of heart mitochondria with physiological ligands, Eur. J. Biochem. 125 (1982) 215–220.
[30] P.A. Rea, J.C. Turner, Tonoplast adenosine triphosphatase and inorganic pyrophosphatase, Methods Plant Biochem. 3 (1990) 385–405.
[31] M.G. Claros, G. von Heijne, TopPred II: an improved software for membrane protein structure predictions, Comput. Appl. Biosci. 10 (1994) 685–686.
[32] E.L.L. Sonnhammer, G. von Heijne, A. Krogh, A hidden Markov model for predicting transmembrane helices in protein sequences, Intell. Syst. Mol. Biol. 6 (1998) 175–182.
[33] G.E. Tusnady, I. Simon, Principles governing amino acid composition of integral membrane proteins: application to topology prediction, J. Mol. Biol. 283 (1998) 489–506.
[34] D.T. Jones, W.R. Taylor, J.M. Thornton, A model recognition approach to the prediction of all-helical membrane protein structure and topology, Biochemistry 33 (1994) 3038–3049.
[35] S. Jayasinghe, K. Hristova, S.H. White, Energetics, stability, and prediction of transmembrane helices, J. Mol. Biol. 312 (2001) 927–934.
[36] H. Knight, A.J. Trewavas, M.R. Knight, Cold calcium signaling in *Arabidopsis* involves two cellular pools and a change in calcium signature after acclimation, Plant Cell 8 (1996) 489–503.
[37] P. Nyrén, B.F. Nore, Å. Strid, Proton-pumping *N*,*N*′-dicyclohexylcarbodiimide-sensitive inorganic pyrophosphate synthase from *Rhodospirillum rubrum*: purification, characterization, and reconstitution, Biochemistry 30 (1991) 2883–2887.
[38] M.G. Palmgren, Acridine orange as a probe for measuring pH gradients across membranes: mechanism and limitations, Anal. Biochem. 192 (1991) 316–321.
[39] P. Nyrén, K. Hajnal, M. Baltscheffsky, Purification of the membrane-bound proton-translocating inorganic pyrophosphatase from *Rhodospirillum rubrum*, Biochim. Biophys. Acta 766 (1984) 630–635.
[40] F. Macrì, M. Zancani, E. Petrussa, P. Dell'Antone, A. Vianello, Pyrophosphate and H^+-pyrophosphatase maintain the vacuolar proton gradient in metabolic inhibitor-treated *Acer pseudoplatanus* cells, Biochim. Biophys. Acta 1229 (1995) 323–328.
[41] S. Clerc, Y. Barenholz, A quantitative model for using acridine orange as a transmembrane pH gradient probe, Anal. Biochem. 259 (1998) 104–111.
[42] T. Bizouarn, M. Althage, A. Pedersen, A. Tigerström, J. Karlsson, C. Johansson, J. Rydström, The organization of the membrane domain and its interaction with the NADP(H)-binding site in proton-translocating transhydrogenase from *E. coli*, Biochim. Biophys. Acta 1555 (2002) 122–127.